

- [9] I. E. Getreu, *Modeling the Bipolar Transistor*. Beaverton, OR: Tektronik, 1976.
- [10] C. R. C., *Handbook of Tables for Mathematics*, 4th ed. Cleveland, OH: Chemical Rubber, 1975.
- [11] F. Fiori and V. Pozzolo, "Modified Gummel-Poon BJT model for electromagnetic susceptibility prediction," in *Proc. Conf. Electromagn. Adv. Applicat.*, Torino, Italy, Sept. 1995, pp. 151–154.
- [12] F. Fiori, T. Foti, and V. Pozzolo, "Computer aided analysis of RF effects in BJT circuits," in *Proc. IEEE Int. Symp. EMC*, Santa Clara, CA, Aug. 1996, pp. 294–299.
- [13] T. I. Quarles, "SPICE3 Version 3C1 Users Guide," Electron. Res. Lab., Univ. California, Berkeley, Rep. ERL-M46, 1989.
- [14] —, "Adding Devices to SPICE3," Electron. Res. Lab., Univ. California, Berkeley, Rep. ERL-M45, 1989.
- [15] —, "The SPICE3 Implementation Guide," Electron. Res. Lab., Univ. California, Berkeley, Rep. ERL-M44, 1989.

## Automated Double-Frequency Testing Technique for Mapping Receiver Interference Responses

Vladimir I. Mordachev

**Abstract**—This paper presents the basic principles of a double-frequency testing technique for highly informative visualization of the linear and nonlinear interference responses of receivers. The technique is implemented with an automated double frequency test system (DFTS) built around conventional controlling and measuring equipment. The main advantages of DFTS are gained by using the principles of raster-like changing of test signals frequencies combined with visualization of test results as two-dimensional (2-D) raster images of the receiver-under-test double-frequency diagrams (or interference response maps). Basic functionalities of the technique for double-frequency testing, which make possible automated detection and identification of all types of interference in the receiver and measurement of their parameters, are described. Results of practical implementation of this technique for testing super-high frequency (SHF) receivers, RF amplifiers (RFA), and diode generator are discussed.

**Index Terms**—Electromagnetic compatibility, intermodulation paths, measurements, nonlinear interference, receiver, spurious response.

### I. INTRODUCTION

A characteristic feature of reception in severe environments is the presence of a number of strong signals at the receiver input. These signals may cause nonlinear effects (blocking, crosstalk, intermodulation, local oscillator noise conversion), and interference in spurious response receiver paths. Since local on-board systems (aircraft and ships) and regional ground-based systems generally must function in severe operational environments, information about standardized electromagnetic compatibility (EMC) characteristics of receivers (typically frequency selectivity characteristic, third-order intercept point, 1-dB compression point, two-signal spurious-free dynamic range, etc.) may be insufficient for EMC analysis and prediction. Developers of collocated radio systems usually have to conduct extensive additional research on susceptibility of receivers. This research involves detection and identification of all possible interference impact paths, evaluation of the interference

effects at the receiver antenna input and measurement of the path and interference characteristics.

The technique for double-frequency testing presented in this paper is a very efficient technique for extracting information about receiver susceptibility at the antenna input [1]–[3]. Unlike widely used techniques based on two- and multisignal testing to determine the electromagnetic compatibility of receivers, this technique permits prompt detection and identification of all existing linear and nonlinear signal paths that cause interference at the receiver antenna input. This technique has been verified over many years of testing by the author as well as by other EMC engineers and it has proved to be highly informative and efficient [4]. The technique is especially useful at the early development stages since it enables the EMC engineer to conduct painstaking research in order to provide detailed data, thus facilitating design decisions.

The technology of "radiolocation" testing of receivers with the use of the technique for double-frequency testing includes the following key stages.

- 1) Detection of all paths and phenomena [which can affect receiver operation under the conditions of specified (predicted) maximum signal levels and over all possible input signal frequencies] including:
  - spurious response paths;
  - paths (types) of two-signal intermodulation;
  - blocking;
  - crosstalk;
  - excitation of input stages under the influence of strong out-of-band signals;
  - locking of the local oscillator frequency by an input signal.
- 2) Identification of spurious response and intermodulation paths as well as other interference effects detected in the receiver.
- 3) Measurement of the parameters and characteristics of the possible interference paths that were detected and identified during the previous two stages.

During the first test stage, the form and cross-sections of the double-frequency amplitude characteristic of the receiver-under-test are analyzed. This characteristic has a dependence

$$H(f_1, f_2) = U_{\text{out}} \left( f_1, f_2 \left| \begin{array}{l} U_{1\text{in}} = \text{const.} \\ U_{2\text{in}} = \text{const.} \end{array} \right. \right) \quad (1)$$

where  $U_{\text{out}}$  is the output signal level when two test signals at frequencies  $f_1$  and  $f_2$  with levels  $U_{1\text{in}}$ ,  $U_{2\text{in}}$  are applied to the receiver input. This stage is completed by recording and displaying in coordinates  $\{f_1, f_2\}$  one or several cross sections of the double-frequency amplitude characteristic

$$W_i(f_1, f_2 | U_{ti}) = \text{sgn}\{H(f_1, f_2) - U_{ti}\} \quad (2)$$

at the specified threshold levels  $U_{ti}$ ,  $i = 1, 2, \dots$ , where the label  $\text{sgn}$  means signum function. These levels are selected so that they exceed the level of the internal noise of the receiver at its output in accordance with the accepted criteria used for determination of the receiver main channel sensitivity and are also selected to test the receiver susceptibility due to spurious response paths and nonlinear effects. Recorded images of cross sections of the double-frequency amplitude characteristic are, in effect, fragments of the known double-frequency diagram of the receiver; examples of such diagrams may be found, for example, in [5] and [6].

The second test stage includes evaluation of the image structure on the double-frequency diagrams (see (2)) and identification of each image component. Image components are line segments and for

Manuscript received September 25, 1998; January 19, 2000.

The author is with the Belarusian State University of Informatics and Radioelectronics, Minsk, 220027 Republic of Belarus (E-mail: nilemc@gw.bsuir.unibel.by).

Publisher Item Identifier S 0018-9375(00)04685-8.

coordinates  $\{f_1, f_2\}$ , the general equation for a single-conversion receiver is as follows:

$$\begin{aligned}
 k_1 f_1 + k_2 f_2 &= k_g f_g + k_{int} f_{int} \\
 k_1, k_2 &= 0, \pm 1, \pm 2, \dots; \quad k_g = 0, 1, 2, \dots; \quad k_{int} = \pm 1 \\
 \min\{|k_1| + |k_2|\} &= 1, \quad L = |k_1| + |k_2|
 \end{aligned}
 \tag{3}$$

where  $f_g$  is the local oscillator voltage frequency,  $f_{int}$  is the intermediate frequency of the receiver,  $L$  is the order of intermodulation oscillation with frequency  $k_1 f_1 + k_2 f_2$  formed by conversion of test signals due to the receiver-under-test nonlinearity.

The third test stage includes measurements to determine the characteristics and parameters (sensitivity, bandwidth, dynamic range) of the detected spurious response and intermodulation paths and to characterize the receiver susceptibility to blocking and crosstalk. During this stage, measurement procedures in accordance with the relevant standards as well as additional measurement procedures can be carried out. Also other measurement procedures can be performed in order to obtain necessary receiver data of consequent EMC analysis and prediction. The measured double-frequency diagrams serve as “topographic maps” or “radiolocation panoramas” and contain information about all the detected paths and effects. These maps or panoramas can be used to perform quantitative analyses. Various measurements can be carried out when signals are tuned to  $f_1$  and  $f_2$  at any point of the double-frequency diagram image.

## II. DFTS STRUCTURE

The basic block diagram of the DFTS is shown in Fig. 1. Key elements of the DFTS are RF signal generators 1, 2, and a computer with a standard interface, e.g., IEEE-488. The computer is used to automatically control the generators and to evaluate signal parameters at the output of the receiver-under-test.

A distinctive feature of the DFTS is how test signals are changed in a line-frame fashion; that is, the frequency  $f_1$  of the first test signal changes at a fast rate and the frequency  $f_2$  of the second test signal changes at a slow rate (or vice versa), which enables one to obtain two-dimensional (2-D) raster images of double-frequency diagrams.

Typical operations performed on the output signal of the receiver-under-test are amplification, detection (in case the signal at the output of the intermediate frequency section of the receiver under test is analyzed), frequency filtering (in case broad-band equipment is tested), comparison to the fixed threshold level  $U_t$ , or multibit analog-to-digital conversion. If necessary, additional modules are included in the DFTS structure, for instance:

- as shown in Fig. 2, an RF signal generator 3 for generation of the valid signal is added, for example, when a coherent receiver is tested;
- equipment for measuring parameters of test signals (frequency, power, and modulation parameters) utilized for initial calibration of the DFTS;
- equipment to measure the output signal (frequency, level, and modulation parameters) in order to perform standard measurements of EMC characteristics and parameters and in order to perform identification and qualitative estimation of nonlinear effects during the tests.

Specialized software is the principal part of the DFTS. This software is used for control of all system elements during the preparatory stage and test stages as well as for processing, storing, and output documenting test data. The software is responsible for implementation of the following crucial operations and functions.

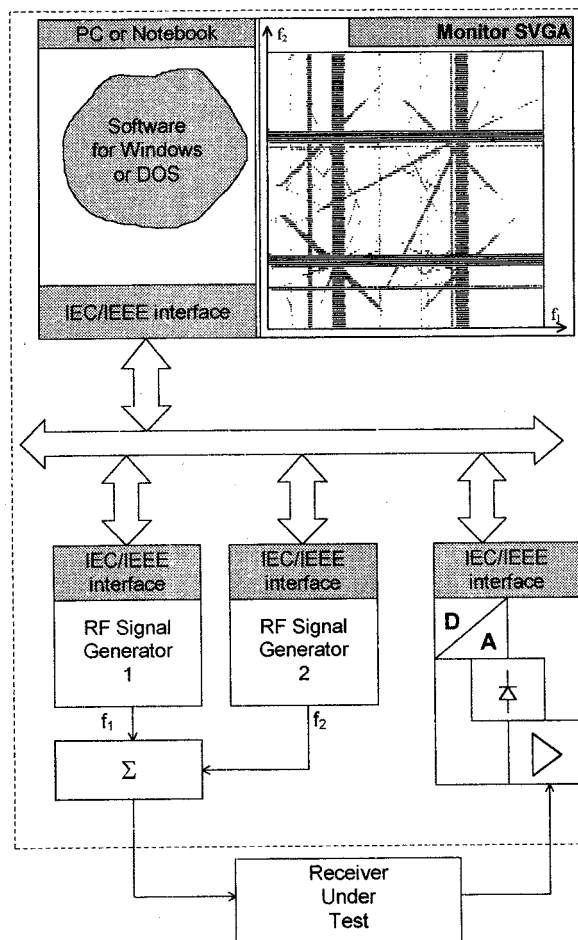


Fig. 1. Basic block diagram of the DFTS.

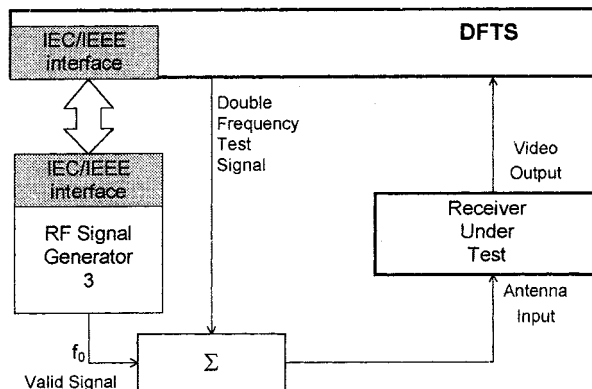


Fig. 2. Double-frequency testing of a coherent receiver.

- Calibration of the DFTS, selection of test signal parameters, and selection of the receiver response conversion parameters.
- Changing test signal frequencies in a raster fashion (100–200 or more lines per frame) in coordinates  $\{f_1, f_2\}$  while synchronously extracting information about the receiver response to test signals in order to create a double-frequency diagram of the receiver.
- Displaying the image of the double-frequency diagram and printing, compressing, and storing data in a database.

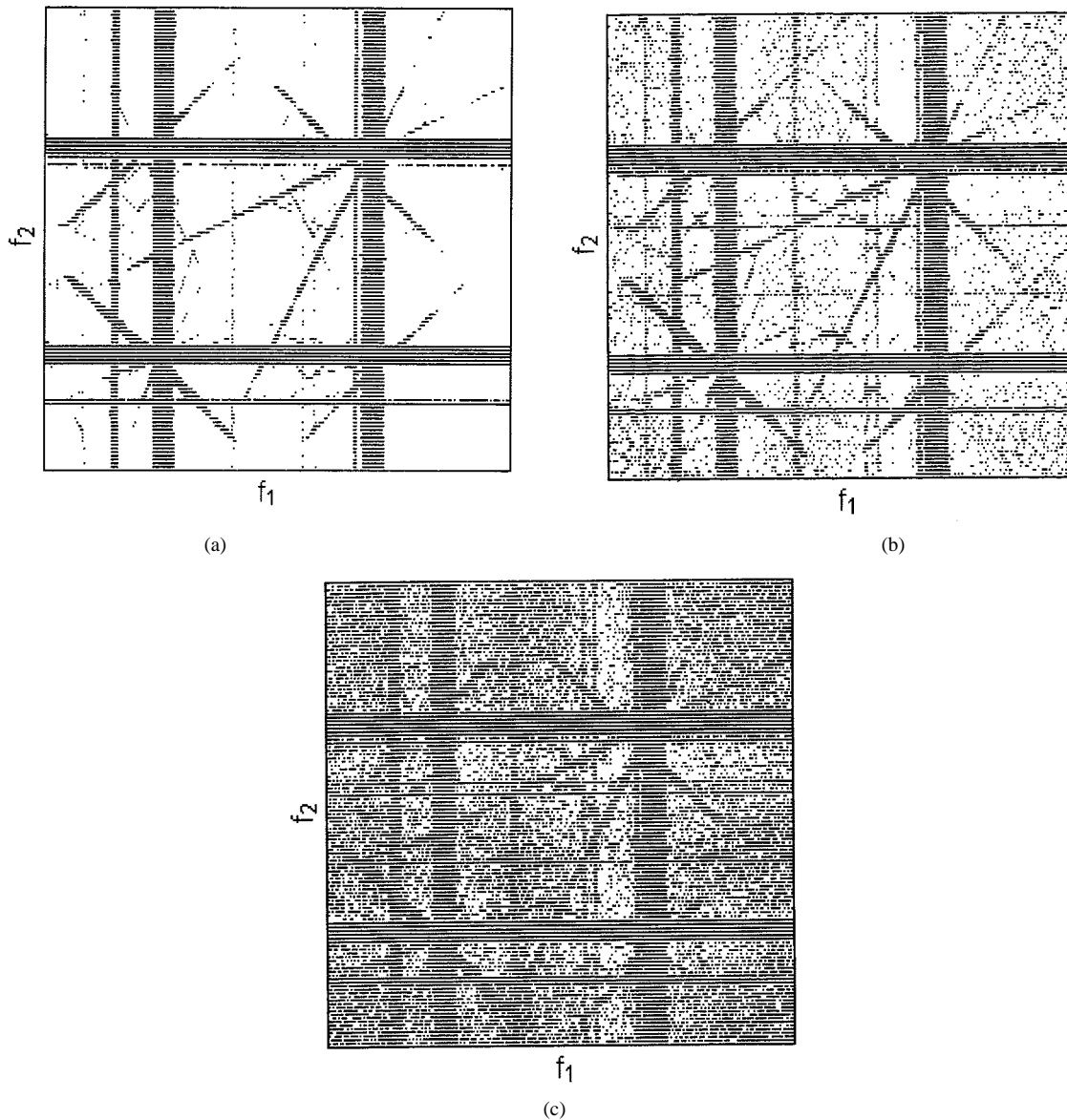


Fig. 3. (a) Double-frequency diagram of a radar receiver for  $U_t/U_N = 15$  dB. (b) Double-frequency diagram of a radar receiver for  $U_t/U_N = 9$  dB. (c) Double-frequency diagram of a radar receiver for  $U_t/U_N = 3$  dB.

- Performing procedures to identify elements of the double-frequency diagram images (including identification of detected spurious response paths and two-signal intermodulation paths).
- Controlling instrumentation during various automatic, semiautomatic, and step-by-step (“manual”) measurements of parameters and characteristics of detected spurious response paths and intermodulation paths as well as of standardized EMC characteristics of the receiver-under-test.
- Executing and managing special databases containing information about parameters and results of tests.

### III. EXAMPLES OF DOUBLE-FREQUENCY RECEIVER TESTING

Fig. 3(a)–(c) shows several images of double-frequency diagrams of a microwave radar receiver for different ratios of threshold level  $U_t$  to noise level  $U_N$  at the receiver output. These double-frequency diagrams contain images of the main receive channel and spurious response paths that look as pairs of lines (one horizontal  $f_2 = \text{const.}$  and one vertical  $f_1 = \text{const.}$ ) crossing on the double-frequency diagram diagonal  $\{f_1 = f_2\}$ . Some of images presented here are cre-

ated by spurious response paths formed by the first local oscillator signal second and third harmonics and by spurious response paths created during the second frequency conversion. Pairs of slanting lines which are symmetric about the diagonal of the double-frequency diagram image represent intermodulation paths. The images shown in these figures reveal the presence of intermodulation oscillations of the second, third, and fifth order which are passed to the receiver output by way of the main receive channel and by spurious response paths including paths created by higher harmonics of local oscillator signals. The techniques for identification of individual images are described in [7]. The basic principles are presented in Section IV. Depending on the complexity of the instrumentation, the DFTS provides various levels of automated images identification, including “paths” of intermodulation detected in the receiver-under-test. When the threshold level  $U_t$  is decreased during receiver response analyses, the ratio  $U_t/U_N$  decreases. This is evident in Fig. 3(a), where  $U_t/U_N = 15$  dB, in Fig. 3(b), where  $U_t/U_N = 9$  dB, and in Fig. 3(c), where  $U_t/U_N = 3$  dB. In Fig. 3(a), notice the decrease in the number of noise outbursts registered on the raster image of the double-frequency diagram. On the one hand, this

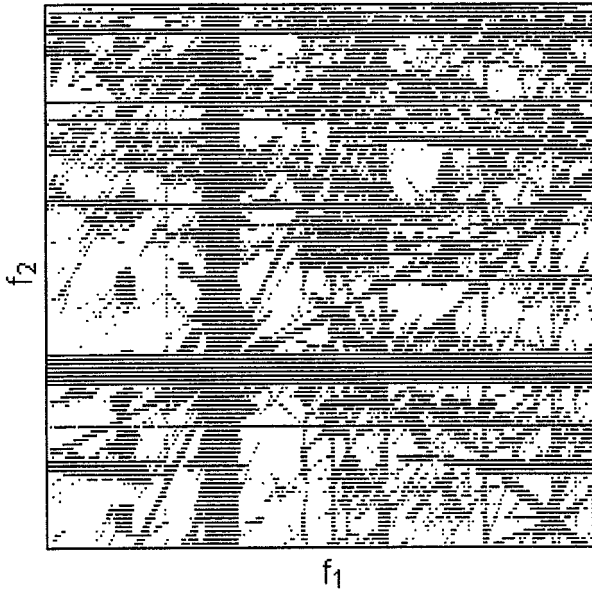


Fig. 4. Double-frequency diagram of a receiver with high-level input.

leads to closer similarity between this receiver response detection technique and conventional radar object/target detection techniques. On the other hand, this is an evidence of the fact that receivers can be tested at small values of the ratio  $U_t/U_N$  due to regular structure of the elements of considered cross sections.

Decreasing the  $U_t/U_N$  ratio to  $3 \cdot 6$  dB has practically no effect on the detection and recognition adequacy of spurious response and intermodulation paths since double-frequency diagram elements and element groups have regular structure. Besides, testing with the use of low values of  $U_t/U_N > 0$  dB makes it possible to display and analyze receiver-under-test responses whose output levels are low and close to the noise level at the receiver output (in particular, to display and analyze high-order intermodulation oscillations and responses on spurious response paths formed by higher harmonics of local oscillator signals). The DFTS may also be used if  $U_t/U_N < 0$  dB, but in this case, known techniques for image detection and recognition in noise environment or additional output signal filtering procedures (for example, additional signal frequency or waveform filtering) should be applied.

Visual representation of double-frequency diagrams to a great extent depends on the test signals levels and the frequency ranges. The double-frequency diagram image shown in Fig. 4 was obtained at test signals levels which exceeded the threshold value of the receiver susceptibility to nonlinear effects (intermodulation) by 24 dB. In this case, a large number of paths (components) of two-signal intermodulation is present on the double-frequency diagram due to these excessive test signal levels and, hence, it is almost impossible to choose compatible frequency combinations of these very strong input signals.

The test procedure using the DFTS is completed by measuring EMC parameters and characteristics of the receiver-under-test. The DFTS system makes it possible to measure both standard and additional EMC parameters and characteristics. Utilization of various system aids (manual control of the system with the use of the cross-hair pointer; automated tuning to the maximum sensitivity of a path or the main receive channel; automated measurement and visualization of the amplitude-frequency characteristic of a particular path; and tuning to the main receive channel, etc.) allows one to measure parameters of every detected path or effect at any point and on any line in the double-frequency diagram. These measurements make it possible to obtain a lot of additional information about signal susceptibility at

the receiver antenna input, which allows one to substantially increase the efficiency of EMC analysis and prediction for radio equipment in close proximity.

#### IV. METHODS FOR IDENTIFICATION OF THE DOUBLE-FREQUENCY DIAGRAM IMAGE COMPONENTS

The problem of identification of spurious response and intermodulation paths detected on the double-frequency diagram is solved by determining the coefficients  $k_1, k_2, k_g, k_{int}$  [see (3)], for each of the identified components. Fig. 5 contains the identification results for a dual-frequency conversion 10-GHz band receiver with no input filters. Sixteen images of spurious response paths and second- to third-order intermodulation paths were identified as a result of this procedure. Possible variants of identification of detected spurious response and intermodulation paths on the basis of the DFTS are enumerated in Fig. 5.

1) *Parameter Identification by Image Location on the Double-Frequency Diagram:* If the considered image is at the angle  $\alpha$  with the abscissa axis then

$$tg(\alpha) = -\frac{G_x k_1}{G_y k_2}; \quad G_x = \frac{Df_1}{Dx}, \quad G_y = \frac{Df_2}{Dy} \quad (4)$$

where  $Df_1, Df_2$  = the bandwidth amount of the frequency change range for the first and second test signals, respectively, [Hz],  $Dx, Dy$  = the horizontal and vertical size of the double-frequency diagram component, respectively, [m],  $G_x, G_y$ —scale of the double-frequency diagram image in horizontal and vertical directions, respectively, [Hz/m].

Each image (line) on the double-frequency diagram is at a certain angle  $\beta$  with the double-frequency diagram diagonal  $\{f_1 = f_2\}$ . Horizontal ( $k_1 = 0$ ) and vertical ( $k_2 = 0$ ) images ( $\beta = 45^\circ$  for  $G_x = G_y$ ) correspond to the main receive channel and spurious response paths, images with other values of  $\beta$  correspond to intermodulation paths. If the scale of the double-frequency diagram is equal in horizontal and in vertical axes then:

- for  $-45^\circ < \beta < 45^\circ$  ( $0^\circ < \alpha < 90^\circ$ ), the coefficients  $k_1, k_2$  have opposite signs, the coefficient whose modulo is of lesser value is negative;
- if intermodulation image crosses the diagonal  $\{f_1 = f_2\}$  from bottom to top ( $0^\circ < \beta < 45^\circ$  or  $45^\circ < \alpha < 90^\circ$ ) then  $k_1 > 0$  and  $k_2 < 0$ , for the symmetrical direction ( $-45^\circ < \beta < 0^\circ$  or  $0^\circ < \alpha < 45^\circ$ ), we have  $k_2 > 0$  and  $k_1 < 0$ ;
- for  $\beta = 0$  ( $\alpha = 45^\circ$ ) we have  $|k_1| = |k_2|, k_1 = -k_2$ ; for  $k_1 > 0$  this line is located below the diagonal of the double-frequency diagram for  $k_2 > 0$ , above the diagonal;
- for  $45^\circ < \beta < 135^\circ$  ( $90^\circ < \alpha < 180^\circ$ ) both coefficients are positive.

If the coordinates  $\{x_1, y_1\}, \{x_2, y_2\}$  of two points on a line are measured on the double-frequency diagram then

$$k_2/k_1 = ((x_1 - x_2)G_x)/((y_2 - y_1)G_y). \quad (5)$$

The information about  $k_g$  may be obtained by comparing the double-frequency diagrams for different tuned frequencies of the receiver-under-test. In particular, if the receiver tuned frequency is changed by a certain value  $\delta f$ , the spurious response path image is displaced in the cross section  $f_2 = \text{const.}$  ( $y = \text{const.}$ ) by the value  $\delta x = \delta f_1/G_x$  and in cross section  $f_1 = \text{const.}$  ( $x = \text{const.}$ ) by the value  $\delta y = \delta f_2/G_y$ , then  $k_g = k_1 \delta f_1 / \delta f = k_2 \delta f_2 / \delta f$ . Finally, if the receiver-under-test is tuned to a different frequency and the location of the considered image (line) has not changed then the corresponding receive channel or spurious response path is formed independently of the local oscillator voltage ( $k_g = 0$ ).

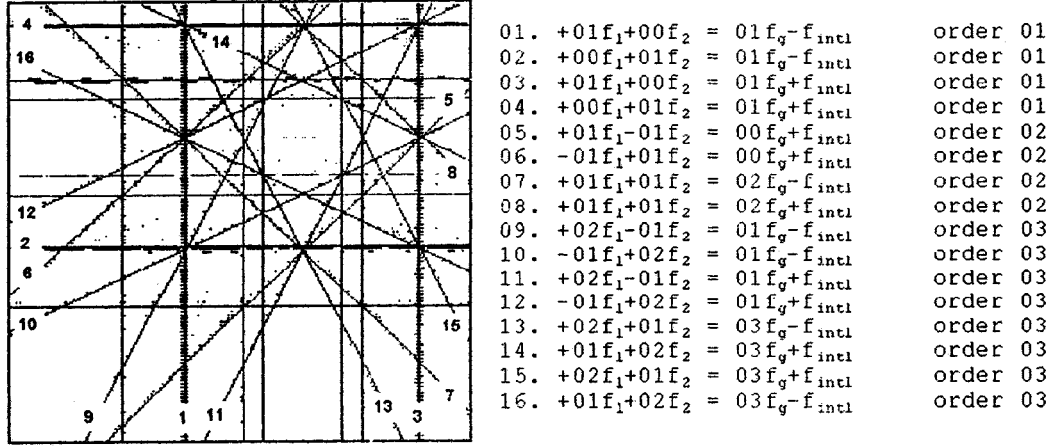


Fig. 5. Results of automated identification of linear and nonlinear paths detected in a radio receiver.

2) *Identification with the Use of the Laws of Relative Location of Receiver Spurious Response and Intermodulation Paths Images:* On the double-frequency diagram of the receiver-under-test, the images of receiver spurious response and intermodulation paths form distinctive (typical) groups; the most frequent of these groups are shown in Fig. 6(a)–(g) (for the typical single-frequency conversion receiver with  $f_g = 10$  GHz,  $k_{int} = -1$ ,  $f_{int} = 1$  GHz), and as described below.

- Groups of spurious response paths images  $k_1f_1 = k_gf_g + k_{int}f_{int}$ ,  $k_2f_2 = k_gf_g + k_{int}f_{int}$  forming typical figures that look like embedded squares whose sides are divisible and parallel to the coordinate axes [see Figs. 5 and 6(a), 6(e)–(g)], and
- Groups of images that form a node of images of the  $L$ th order on the double-frequency diagram diagonal  $\{f_1 = f_2\}$  in the point  $Lf_1 = Lf_2 = k_gf_g + k_{int}f_{int}$ . This node of images includes
  - horizontal and vertical images of the spurious response path  $k_1f_1 = k_2f_2 = k_gf_g + k_{int}f_{int}$ ,  $k_1 = k_2 = L$ ;
  - $L-1$  images of the intermodulation paths  $k_1f_1 + k_2f_2$  with the coefficients  $k_1 > 0$ ,  $k_2 > 0$ ;  $k_1 + k_2 = L$ , that are at the angle  $\pi/4 < \beta \leq \pi/2$  about the diagonal  $\{f_1 = f_2\}$ ;
  - pairs of the intermodulation paths images of the type  $(L+m)f_{1,2} - mf_{2,1} = k_gf_g + k_{int}f_{int}$  and order  $L_m = L + 2m$  that are symmetric about the double-frequency diagram diagonal  $\{f_1 = f_2\}$ ,  $m = 1, 2, \dots$ .

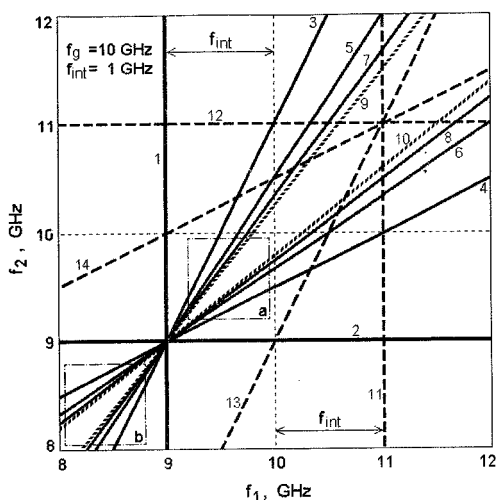
Fig. 6(a)–(d) shows typical and most common image nodes of first to fourth order. These image groups can be easily identified on double-frequency diagrams produced during actual tests and are shown in Figs. 3–5, 7, and 12. The image group shown in Fig. 6(a) (node of the first order formed by lines 1–10) is the most common image group because it is created primarily by the main receive channel and most dangerous intermodulation types. The crosspoints (nodes) of images under consideration are situated horizontally and vertically at the distance  $\Delta f_1(L, k_{int}) = \Delta f_2(L, k_{int}) = k_{int}f_{int}/L$  from the point with the coordinates  $\{f_1 = f_g, f_2 = f_g\}$ . Coordinates of the  $i$ th and  $j$ -th nodes having parameters  $\{L_i, k_{int i}\}$  and  $\{L_j, k_{int j}\}$  differ correspondingly by the value of  $f_{int}(k_{int i}/L_i - k_{int j}/L_j)$ ;

- groups of images of the intermodulation paths of the type  $m(f_{1,2} - f_{2,1}) = f_{int}$ ,  $m = 1, 2, \dots$  and order  $L = 2m$  represented by lines that are parallel to the double-frequency

diagonal  $\{f_1 = f_2\}$  and are located at distances  $\Delta x = f_{int}/mG_x$ ,  $\Delta y = f_{int}/mG_y$  for axes  $X, Y$  from this diagonal [see Fig. 6(e)].

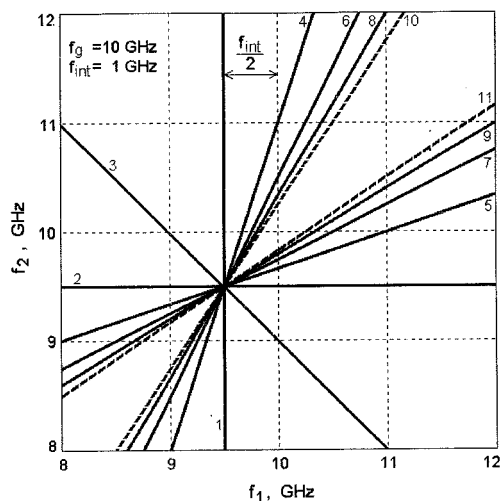
On the double-frequency diagrams of some kinds of receivers-under-test, the above mentioned typical groups of receiver spurious response and intermodulation paths images form distinctive (typical) image compositions; some of the most frequent of these compositions are contained on examples in Figs. 6(f), (g), 7, and 8 and described below.

- 1) Double-frequency diagram for a superheterodyne receiver with an input parametric RF amplifier (RFA) typically [besides the typical image node formed by the main receive channel and odd-order intermodulation and shown in Fig. 6(a) and the image group formed by even-order intermodulation of the type  $m(f_{1,2} - f_{2,1}) = f_{int}$ ,  $m = 1, 2, \dots$  and shown in Fig. 6(e)] includes a number of specific image groups [see Fig. 6(f)]: a group of intermodulation images  $(m+1)f_{1,2} - mf_{2,1} = k_{int}f_{int}$ , which are formed directly by penetration of intermodulation components into the intermediate frequency band [lines 11–18 on Fig. 6(f)], and two second-order nodes of intermodulation images formed by participation of RFA pump voltage with frequency  $f_p = 2(f_g + k_{int}f_{int})$  [dot lines 5–10 on Fig. 6(f)]. By and large, the author believes that images shown in Fig. 6(a), (e), and (f) sufficiently facilitate visual identification of experiment results shown in Fig. 7, which contains a double-frequency diagram for a 10-GHz-band receiver with an input parametric RFA. A characteristic feature of this double-frequency diagram is the presence of a large number of high-order intermodulation paths, which are created directly by penetration of intermodulation components into the intermediate frequency band [ $k_g = 0$  in (3)]. These paths are represented as pairs of slanting lines placed symmetrically about the diagonal of the double-frequency diagram in the top left and bottom right quadrants of the image shown in Fig. 7. Presence of these paths at a substantial distance from the tuned frequency of the receiver means that the resonance circuit of the particular receiver-under-test parametric RFA practically does not suppress nonlinear spectral components created due to the influence of strong signals on the amplifier. Similar images are created by a



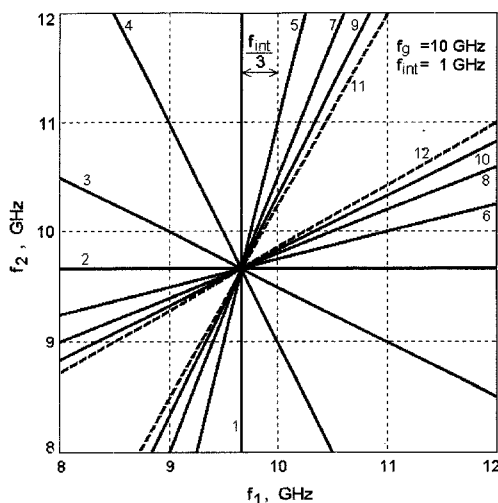
No	Type	Order	No	Type	Order
1.	$f_1 = f_g - f_{int}$	1	8.	$4f_2 - 3f_1 = f_g - f_{int}$	7
2.	$f_2 = f_g + f_{int}$	1	9.	$(m+1)f_1 - mf_2 = f_g - f_{int}$	$2m+1$
3.	$2f_1 - f_2 = f_g - f_{int}$	3	10.	$(m+1)f_2 - mf_1 = f_g - f_{int}$	$2m+1$
4.	$2f_2 - f_1 = f_g - f_{int}$	3	11.	$f_1 = f_g + f_{int}$	1
5.	$3f_1 - 2f_2 = f_g - f_{int}$	5	12.	$f_2 = f_g + f_{int}$	1
6.	$3f_2 - 2f_1 = f_g - f_{int}$	5	13.	$2f_1 - f_2 = f_g + f_{int}$	3
7.	$4f_1 - 3f_2 = f_g - f_{int}$	7	14.	$2f_2 - f_1 = f_g + f_{int}$	3

(a)



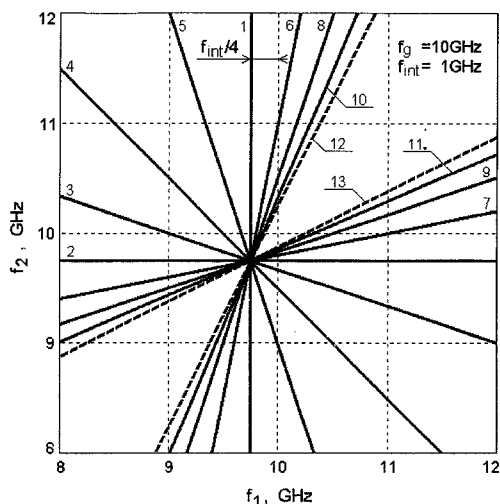
No	Type	Order	No	Type	Order
1.	$2f_1 - 2f_2 = f_g - f_{int}$	2	7.	$4f_2 - 2f_1 = 2f_g - f_{int}$	6
2.	$2f_2 = 2f_1 + f_g - f_{int}$	2	8.	$5f_1 - 3f_2 = 2f_g - f_{int}$	8
3.	$f_1 + f_2 = 2f_g - f_{int}$	2	9.	$5f_2 - 3f_1 = 2f_g - f_{int}$	8
4.	$3f_1 - f_2 = 2f_g - f_{int}$	4	10.	$(m+2)f_1 - mf_2 = 2f_g - f_{int}$	$2m+2$
5.	$3f_2 - f_1 = 2f_g - f_{int}$	4	11.	$(m+2)f_2 - mf_1 = 2f_g - f_{int}$	$2m+2$
6.	$4f_1 - 2f_2 = 2f_g - f_{int}$	6			

(b)



No	Type	Order	No	Type	Order
1.	$3f_1 = 3f_2 - f_g - f_{int}$	3	7.	$5f_1 - 2f_2 = 3f_g - f_{int}$	7
2.	$3f_2 = 3f_1 - f_g - f_{int}$	3	8.	$5f_2 - 2f_1 = 3f_g - f_{int}$	7
3.	$2f_2 + f_1 = 3f_g - f_{int}$	3	9.	$6f_1 - 3f_2 = 3f_g - f_{int}$	9
4.	$2f_1 + f_2 = 3f_g - f_{int}$	3	10.	$6f_2 - 3f_1 = 3f_g - f_{int}$	9
5.	$4f_1 - f_2 = 3f_g - f_{int}$	5	11.	$(m+3)f_1 - mf_2 = 3f_g - f_{int}$	$2m+3$
6.	$4f_2 - f_1 = 3f_g - f_{int}$	5	12.	$(m+3)f_2 - mf_1 = 3f_g - f_{int}$	$2m+3$

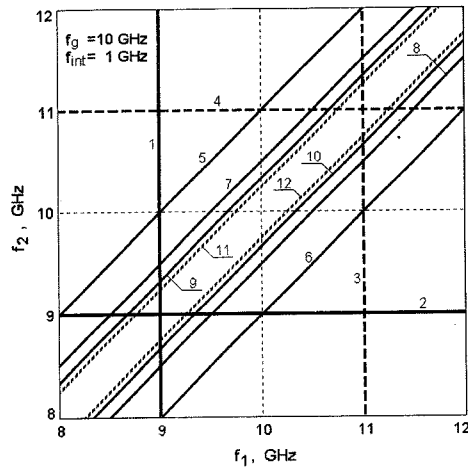
(c)



No	Type	Order	No	Type	Order
1.	$4f_1 = 4f_2 - f_g - f_{int}$	4	8.	$6f_1 - 2f_2 = 4f_g - f_{int}$	8
2.	$4f_2 = 4f_1 - f_g - f_{int}$	4	9.	$6f_2 - 2f_1 = 4f_g - f_{int}$	8
3.	$3f_2 + f_1 = 4f_g - f_{int}$	4	10.	$7f_1 - 3f_2 = 4f_g - f_{int}$	10
4.	$2f_1 + 2f_2 = 4f_g - f_{int}$	4	11.	$7f_2 - 3f_1 = 4f_g - f_{int}$	10
5.	$3f_1 + f_2 = 4f_g - f_{int}$	4	12.	$(m+4)f_1 - mf_2 = 4f_g - f_{int}$	$2m+4$
6.	$5f_1 - f_2 = 4f_g - f_{int}$	6	13.	$(m+4)f_2 - mf_1 = 4f_g - f_{int}$	$2m+4$
7.	$5f_2 - f_1 = 4f_g - f_{int}$	6			

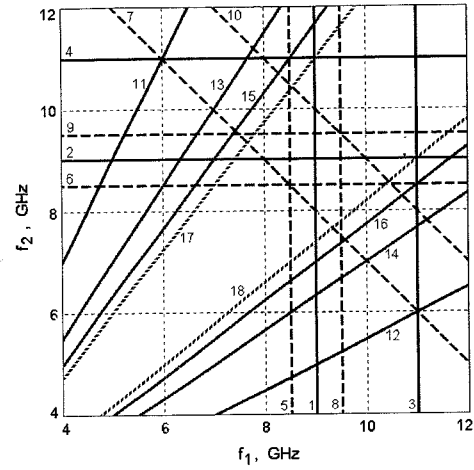
(d)

Fig. 6. (a) The first-order node, the most common node since it contains images formed by the main receive channel (lines 1 and 2). This node is formed by intermodulation, receive channel and spurious response images of the following types. (b) The second-order node, which is formed with the contribution of the local oscillator signal second harmonic and contains intermodulation and spurious response path images of the following types. (c) The third-order node, which is formed with the contribution of the local oscillator signal third harmonic and contains intermodulation and spurious response path images of the following types. (d) The fourth-order node, which is formed with the contribution of the local oscillator signal fourth harmonic and contains intermodulation and spurious response path images of the following types.



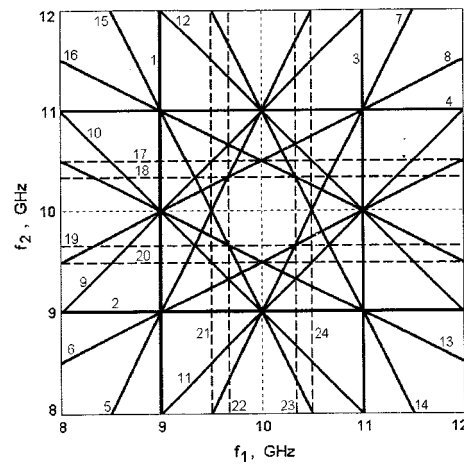
No	Type	Order
1.	$f_1 = f_g - f_{int}$	1
2.	$f_2 = f_g - f_{int}$	1
3.	$f_1 = f_g + f_{int}$	1
4.	$f_2 = f_g + f_{int}$	1
5.	$f_2 - f_1 = f_{int}$	2m
6.	$f_1 - f_2 = f_{int}$	2
7.	$2f_2 - 2f_1 = f_{int}$	4
8.	$2f_1 - 2f_2 = f_{int}$	4
9.	$3f_2 - 3f_1 = f_{int}$	6
10.	$3f_1 - 3f_2 = f_{int}$	6
11.	$mf_2 - mf_1 = f_{int}$	2m
12.	$mf_1 - mf_2 = f_{int}$	2m

(e)



No	Type	Order
1.	$f_1 = f_g - f_{int}$	1
2.	$f_2 = f_g - f_{int}$	1
3.	$f_1 = f_g + f_{int}$	1
4.	$f_2 = f_g + f_{int}$	1
5.	$2f_1 = 2f_g - f_{int}$	2
6.	$2f_2 = 2f_g - f_{int}$	2
7.	$f_1 + f_2 = 2f_g - f_{int}$	2
8.	$2f_1 = 2f_g + f_{int}$	2
9.	$2f_2 = 2f_g + f_{int}$	2
10.	$f_2 + f_1 = 2f_g + f_{int}$	2
11.	$2f_1 - f_2 = f_{int}$	3
12.	$2f_2 - f_1 = f_{int}$	3
13.	$3f_1 - 2f_2 = f_{int}$	5
14.	$3f_2 - 2f_1 = f_{int}$	5
15.	$4f_1 - 3f_2 = f_{int}$	7
16.	$4f_2 - 3f_1 = f_{int}$	7
17.	$(m+1)f_1 - mf_2 = f_{int}$	2m+1
18.	$(m+1)f_2 - mf_1 = f_{int}$	2m+1

(f)



No	Type	Order
1.	$f_1 = f_g - f_{int}$	1
2.	$f_2 = f_g - f_{int}$	1
3.	$f_1 = f_g + f_{int}$	1
4.	$f_2 = f_g + f_{int}$	1
5.	$2f_1 - f_2 = f_g - f_{int}$	3
6.	$2f_2 - f_1 = f_g - f_{int}$	3
7.	$2f_1 - f_2 = f_g + f_{int}$	3
8.	$2f_2 - f_1 = f_g + f_{int}$	3
9.	$f_2 - f_1 = f_{int}$	2
10.	$f_1 + f_2 = 2f_g - f_{int}$	2
11.	$f_1 - f_2 = f_{int}$	2
12.	$f_1 + f_2 = 2f_g + f_{int}$	2
13.	$2f_2 + f_1 = 3f_g - f_{int}$	3
14.	$2f_1 + f_2 = 3f_g - f_{int}$	3
15.	$2f_1 + f_2 = 3f_g + f_{int}$	3
16.	$2f_2 + f_1 = 3f_g + f_{int}$	3
17.	$2f_2 = 2f_g + f_{int}$	2
18.	$3f_2 = 3f_g + f_{int}$	3
19.	$3f_2 = 3f_g - f_{int}$	3
20.	$2f_2 = 2f_g - f_{int}$	2
21.	$2f_1 = 2f_g - f_{int}$	2
22.	$3f_1 = 3f_g - f_{int}$	3
23.	$3f_1 = 3f_g + f_{int}$	3
24.	$2f_1 = 2f_g + f_{int}$	2

(g)

Fig. 6. (Continued.) (e) A typical group of images formed by even-order intermodulation due to direct passage of test signals nonlinear conversion products to the intermediate frequency path. This figure shows intermodulation and receive path images of the following types. (f) A typical group of images formed by intermodulation and spurious response paths present in a superheterodyne receiver with a parametric RFA. This group contains the following images. (g) A typical group of images formed by intermodulation and spurious response paths present in a superheterodyne receiver with a mixer at its input. This group contains the following images.

receiver with electronically controlled input frequency-selective circuits with varicaps.

- 2) Double-frequency diagram for a superheterodyne receiver with an input mixer, as a rule, has a specific structure shown in Fig. 6(g). This structure is one of the most common structures observed in practice since it is formed by images created by the main and image receive channels as well as images created by intermodulation whose order is not higher than the third order. It can easily be observed that this diagram contains typical image nodes of first to third order and typical images created by intermodulation  $f_{1,2} - f_{2,1} = f_{\text{int}}$ , shown in Fig. 6(a)–(c), (e). The similarity of double-frequency diagrams for superheterodyne receivers with dual- and single-frequency conversion [see Figs. 5 and 6(g)] can be explained by the fact that the dual conversion receiver-under-test employs efficient frequency filters that suppress spurious response paths for the second intermediate frequency.
- 3) Fig. 8 shows a double-frequency diagram image of the UHF direct conversion (RF-to-DC) radio receiver with  $f_{\text{int}} = 0$ . The main peculiarities of the double-frequency diagram for this receiver type are as follows:
  - the coordinates of the image nodes shown in Fig. 6(a)–(d) coincide—lines of all the nodes cross at the point  $\{f_1 = f_g, f_2 = f_g\}$ , which corresponds to the receiver tuned frequency.
  - The group of images created by even-order intermodulation and shown in Fig. 6(e) degenerate into the line  $\{f_1 = f_2\}$ , which corresponds to the double-frequency diagram diagonal.

The groups enumerated above do not represent a comprehensive description of all typical variants of relative location of linear and nonlinear paths of signals passage to the receiver output. However, these groups comprise most of the images usually generated in double-frequency diagrams for superheterodyne receivers. By and large, such systematization of double-frequency diagram elements enables one to carry out significantly more efficient and accurate visual identification of images. A training set of typical double-frequency diagrams may be created to aid computer-based automatization of the identification process.

3) *Identification on the Basis of Measurement of Test Signals Values, of Values of  $n$  Frequencies of the Local Oscillator Signals, and of the Signal Value at the Last Intermediate Frequency of the Receiver-Under-Test* ( $f_1, f_2, f_{g1}, \dots, f_{gn}, f_{\text{int}}$ ): Identification of the considered images on the basis of the results of these measurements (for three points that belong to a line on the double-frequency diagram when the single frequency conversion superheterodyne receiver is tested) implies solution of the following system:

$$\left. \begin{aligned} z_1 f_{11} + z_2 f_{21} + z_3 f_{g1} &= f_{\text{int}1} \\ z_1 f_{12} + z_2 f_{22} + z_3 f_{g2} &= f_{\text{int}2} \\ z_1 f_{13} + z_2 f_{23} + z_3 f_{g3} &= f_{\text{int}3} \end{aligned} \right\} \quad (6)$$

$$z_1 = \frac{k_1}{k_{\text{int}}}, \quad z_2 = \frac{k_2}{k_{\text{int}}}, \quad z_3 = -\frac{k_g}{k_{\text{int}}}$$

where  $f_{1i}, f_{2i}, f_{gi}, f_{\text{int}i}$  = results of frequency measurements for  $i$ th point of an image. This technique is easily automated and can be implemented as a background computer calculation task. However, it generally requires simultaneous measurement of values of frequencies identified above for each  $i$ th point of the image in order to decrease the influence on the estimation accuracy of values  $z_1, z_2, z_3$  due to instability of these frequencies. It is clear that the use of this technique for

identification of images obtained while testing an  $n$  frequency conversion receiver implies measurement of test signals values, measurement of values of  $n$  frequencies of the local oscillator signals and measurement of the signal value at the last intermediate frequency of the receiver-under-test in  $n + 2$  points of each identified image created by intermodulation and in  $n + 1$  points of each identified image created by the spurious response path.

4) *Identification on the Basis of Comparison of Test Signals Modulation (Keying) Parameters and Signal Modulation (Keying) Parameters at the Receiver Intermediate Frequency Output*: Implementation of this technique requires the angle modulation (keying) on at least one of the test signals. If this signal (for example, with the frequency  $f_1$ ) undergoes phase shift keying with an angle  $\Delta\varphi_1$  or frequency shift keying with the deviation  $\delta f_1$ , which is not wider than the bandwidth of the studied receiver channel or path, then the parameters of angle modulation of signals at the receiver input and output ( $\Delta\varphi_{\text{int}}, \delta f_{\text{int}}$  for the intermediate frequency output) are in the following simple relationship:

$$|k_1| = \Delta\varphi_{\text{int}}/\Delta\varphi_1 \quad \text{or} \quad |k_1| = \delta f_{\text{int}}/\delta f_1. \quad (7)$$

This can be easily explained by the following. When a nonlinear element is influenced by two harmonic oscillations having amplitudes  $U_1, U_2$ , and phases  $\Phi_1(t) = 2\pi f_1 t + \varphi_1$  and  $\Phi_2(t) = 2\pi f_2 t + \varphi_2$  ( $\varphi_1$  and  $\varphi_2$ —initial oscillation phases) the phase of an intermodulation oscillation of the type  $k_1 f_1 + k_2 f_2$  at the element output will equal  $\Phi_{k_1 f_1 + k_2 f_2}(t) = k_1 \Phi_1(t) + k_2 \Phi_2(t) + \Delta\Psi(U_1, U_2, f_1, f_2)$ , where  $\Delta\Psi(U_1, U_2, f_1, f_2)$  is the output oscillation phase shift caused by the AM/PM conversion  $t$  is the time. Thus

- when the first harmonic test signal phase is changed by  $\Delta\varphi_1$ , we have  $\Phi_1(t) = 2\pi f_1 t + (\varphi_1 + \Delta\varphi_1)$ , and the intermodulation oscillation phase is defined as  $\Phi_{k_1 f_1 + k_2 f_2}(t) = 2\pi(k_1 f_1 + k_2 f_2)t + (k_1 \varphi_1 + k_2 \varphi_2 + k_1 \Delta\varphi_1) + \Delta\Psi(U_1, U_2, f_1, f_2)$ , where  $k_1 \Delta\varphi_1$  is the output oscillation phase shift keying parameter. This parameter is proportional to the desired coefficient  $k_1$ ; it is obvious that if the phase shift keying is used we have to ensure the uniqueness of solution, for example, by using  $\Delta\varphi_1 \ll \pi$ ;
- when the first harmonic test signal frequency is changed by  $\delta f_1$ , we have  $\Phi_1(t) = 2\pi(f_1 + \delta f_1)t + \varphi_1$  and the intermodulation oscillation phase is defined as  $\Phi_{k_1 f_1 + k_2 f_2}(t) = 2\pi(k_1 f_1 + k_2 f_2 + k_1 \delta f_1)t + (k_1 \varphi_1 + k_2 \varphi_2) + \Delta\Psi(U_1, U_2, f_1, f_2)$ , where  $k_1 \delta f_1$  is the output oscillation frequency shift keying parameter; this parameter is proportional to the desired coefficient  $k_1$ ;
- for linear variation of the frequency  $f_1$  of the first harmonic test signal at the rate of  $V_f$ , we have  $\Phi_1(t) = 2\pi(f_1 + V_f t)t + \varphi_1$ , and the intermodulation oscillation phase is defined as  $\Phi_{k_1 f_1 + k_2 f_2}(t) = 2\pi(k_1 f_1 + k_2 f_2 + k_1 V_f t)t + (k_1 \varphi_1 + k_2 \varphi_2) + \Delta\Psi(U_1, U_2, f_1, f_2)$ , where  $k_1 V_f$ —linear variation rate of the output oscillation frequency; this linear variation rate is proportional to the desired coefficient  $k_1$ . Possible ways to use this fact for identification of a receiver-under-test are considered in more detail below.

5) *Identification on the Basis of Comparison of the Frequency Change Rate of the Fast-Changed Test Signal and Frequency Change Rate of the Receiver Response Signal to the Test Signal at the Intermediate Frequency*: The process of receiver testing with the use of the double-frequency testing technique implies fast change of the test signal having frequency  $f_1$  in the bandwidth  $Df_1$  at a rate  $V_f$ . For the case of test signal passage to the receiver output via the channel (path) [see (3)] the output signal change rate equals  $V_{\text{out}} = k_1 \cdot V_f$ . If the DFTS is implemented in the analog mode which provides continuous change of test signals frequencies [1], the use of known measuring equipment for measuring the linearly modulated signal frequency

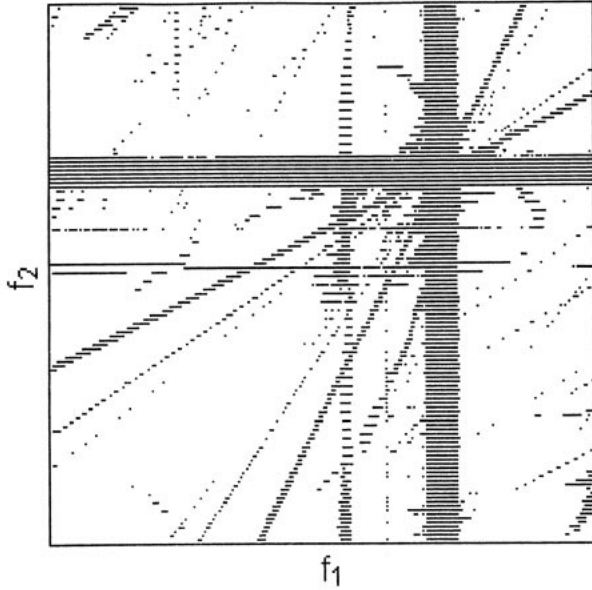
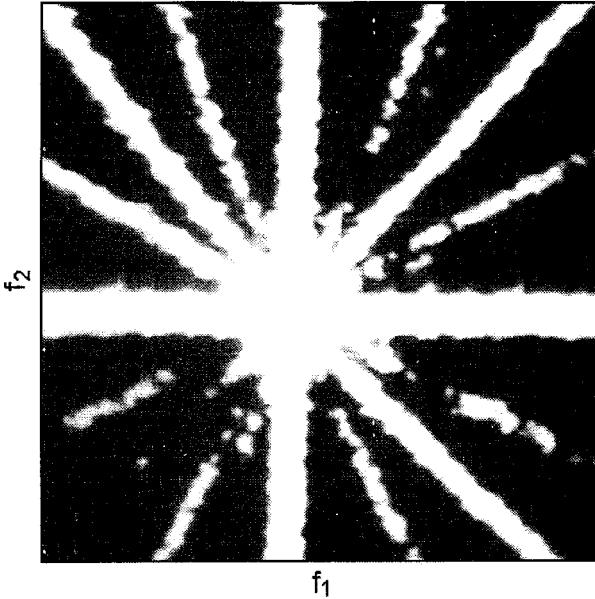
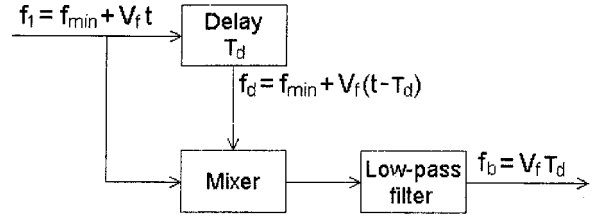


Fig. 7. Double-frequency diagram for a receiver with a parametric RFA.


 Fig. 8. Double-frequency diagram of a RF-to-DC radio receiver ( $f_{\text{int}} = 0$ ).

change rate implemented on the basis of the delay lines [10] provides the capability for automated identification of images immediately during the generation of the receiver double-frequency diagram.

Fig. 9 shows the simplest block diagram of a device that makes it possible to measure the parameter  $V_f$ . Filtering of low-frequency components of the signal which is a product of a signal with linear varying frequency  $f_1 = f_{\text{min}} + V_f t$  and of the signal's copy delayed by  $T_d$  whose frequency is  $f_1 = f_{\text{min}} + V_f(t - T_d)$ , makes it possible to form


 Fig. 9. Block diagram of a device for beat signal generation. The beat signal frequency  $f_b$  is proportional to the input signal frequency sweeping rate  $V_f$ .

a signal with the beat frequency  $f_b = V_f T_d$  which is proportional to the parameter  $V_f$ . When this device is connected to the receiver-under-test intermediate frequency output, the intermodulation signal of the type  $k_1 f_1 + k_2 f_2$  will form the signal with the beat frequency  $f_{b \text{ im}} = |k_1| V_f T_d$ .

The delay time of the signal at the output of the intermediate frequency section of the receiver-under-test  $T_{d \text{ out}}$  (which facilitates formation of not less than  $K$  periods of oscillation of difference frequency (beat signal) at the output of the equipment measuring the magnitude  $V_{\text{out}}$  if the intermodulation oscillation with the frequency  $k_1 f_1 + k_2 f_2$  falls into the passband  $\Delta f$  of the receiver-under-test) is determined by the relationship

$$T_{d \text{ out}} = 2KJ/(|k_1|\Delta f), \quad J = \max\{|k_1|\}. \quad (8)$$

The relationship given by (8) determines the structure of the device for estimation of the values of  $|k_1|$ . The relationship is implemented using multichannel equipment for measuring of  $V_{\text{out}}$  on the basis of the multidrop delay line, which is used to determine the number of the path containing the beat signal with the frequency  $\Delta f/2$ .

A simplified variant of this technique can be implemented by direct measurement and comparison of values of  $V_f$ ,  $V_{\text{out}}$  when the change rate for the test signal frequency  $f_1$  is  $V_f \approx 0.1\Delta f^2/J$  and the delay of the receiver-under-test intermediate frequency signal is  $T_{d \text{ out}} \approx 5/\Delta f$ . In this case, the duration of intermodulation signal present in the intermediate frequency section of the receiver-under-test is  $t_{\text{int}}(k_1) \approx 10J/(|k_1|\Delta f) \gg T_{d \text{ out}}$  and the period of beat signal oscillation at the output of the measuring equipment is  $T_{b \text{ im}} = 1/f_{b \text{ im}} \approx t_{\text{int}}(k_1)/5$  for any  $|k_1| < J$ . To measure  $T_{b \text{ im}}$ , it is quite sufficient to form at the output of the device shown in Fig. 9(a) radio pulse whose duration is  $t_{\text{int}}(k_1)$  and which contains no less than three to four full beat oscillation periods.

Due to the fact that double-frequency diagram is symmetric about the diagonal  $\{f_1 = f_2\}$ , the obtained value  $|k_1| = V_{\text{out}}/V_f$  for one of the symmetric images is equal to the value  $|k_2|$  of the other symmetric images, which facilitates their complete identification by means of the described technique.

Taking into account the possibilities for identification of double-frequency diagrams described above, some results of testing of a receiver shown in Figs. 3–5, 7, 8 prove that the DFTS is very efficient in detection and identification of spurious response and intermodulation paths present in a receiver that operates in severe electromagnetic environment. These results illustrate the capability to study the peculiarities inherent in receivers with various structures.

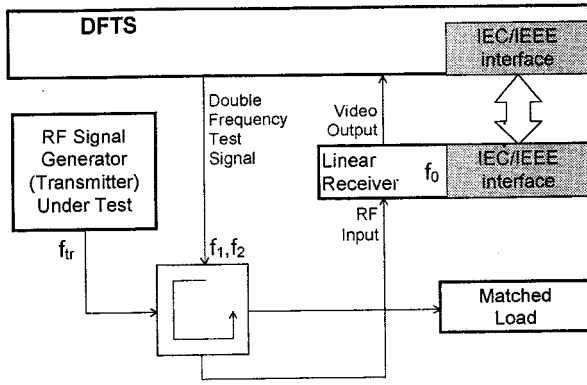


Fig. 10. Double-frequency testing of RF signal generator or transmitter.

## V. ADDITIONAL FUNCTIONALITIES OF DFTS

### A. Testing of Radiotransmitters and RF Generators for Susceptibility to Nonlinear Effects

The double-frequency testing principle can be utilized to study intermodulation oscillation processes formation in RF generators and radiotransmitters. The following conditions must be met to implement these tests.

- The test signal levels shall be close to the signal level at the output of the generator-under-test (transmitter) and test signal frequency change ranges shall include domains of maximum susceptibility.
- Isolating elements (isolators, circulators etc.) and frequency-selective elements (filters) shall be used in order to protect the test signal generators outputs from strong signals of the tested device. Attenuators are also required to reduce the signal level prior to its passage to the linear receiver output so as to enable detection and registration of comparatively low-level intermodulation oscillations.

Intermodulation oscillation frequencies  $f_{IM}(k_1, k_2, k_{tr})$  are related to frequencies  $f_1, f_2, f_{tr}$  of signals participating in intermodulation formation by the following linear equation with integer coefficients:

$$\begin{aligned} k_1 f_1 + k_2 f_2 + k_{tr} f_{tr} &= f_{IM}(k_1, k_2, k_{tr}); \\ k_1, k_2, k_{tr} &= 0, \pm 1, \pm 2, \dots; \\ \min\{|k_1| + |k_2| + |k_{tr}|\} &= 2. \end{aligned} \quad (9)$$

Fig. 10 shows the basic block diagram of the test configuration for double-frequency testing of RF generators. If an intermodulation oscillation falls into the passband of the registering linear receiver tuned to the frequency  $f_0$  and the level of this oscillation exceeds the receiver sensitivity this oscillation is registered as the corresponding graphic line element of the double-frequency diagram image.

Fig. 11 presents the results of double-frequency testing of an IMPATT (impact avalanche and transit time) diode generator [1], [3]. Testing was conducted under the following conditions.

- The IMPATT diode generator-under-test provided oscillation generation at the frequency 8.4 GHz.
- The analogue DFTS generated two test signals whose levels equaled  $-10$  dB with respect to the IMPATT diode generator signal and underwent linear frequency modulation in the frequency ranges  $Df_1 = Df_2 = [8.9 \dots 9.5]$  GHz.
- The linear receiver utilized as the registering device was tuned to fixed frequencies in the range  $f_0 \in [8.5 \dots 8.8]$  GHz.

Some very interesting results were obtained under these conditions. In particular, intermodulation oscillations were registered in the IM-

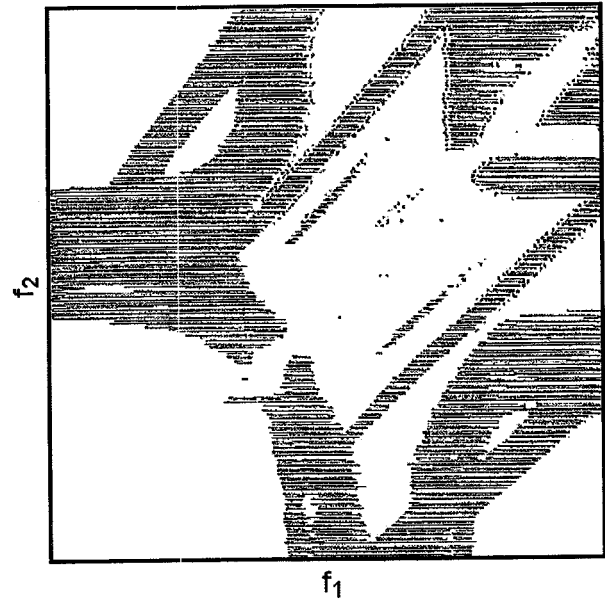


Fig. 11. Double-frequency diagram for an IMPATT diode generator showing nonlinear dependence of frequencies of some intermodulation oscillations on test signal frequencies  $f_1, f_2$ .

PATT diode generator whose frequencies had *nonlinear dependence* on frequencies  $f_1, f_2$  of the test signals (their images are shown as hyperbolas in Fig. 11). These intermodulation oscillations were registered simultaneously with the usual intermodulation oscillations whose images are straight lines that are parallel to the double-frequency diagram diagonal and cross the “anomalous” curves.

The reason for this anomaly is related to the fact that under the influence of the test signals, a spurious noise oscillation that causes the “anomalous” intermodulation oscillations is present in the IMPATT diode generator-under-test output oscillation spectrum. The frequency of this spurious noise oscillation depends on the frequencies of test signals.

The abovementioned nonlinear dependence effect is an evidence of the fact that cases are possible when the conventional linear frequency intermodulation analysis does not provide perfectly reliable prediction of all the possible intermodulation oscillations frequencies.

### B. Testing of Nonlinear Two-Port Radio Devices (Amplifiers and RF Converters)

The double-frequency testing technique of two-port devices is implemented using the configuration shown in Fig. 12. The filter and attenuator shown ensure the radioreceiver operation in the linear mode and ensure matching of the two-port device output and the linear receiver input noise levels. Similarly, to the case shown in Fig. 10, the radioreceiver in the diagram shown in Fig. 12 provides detection and registration of low-level intermodulation oscillations. Measurement of oscillation parameters makes it possible to identify the character of the two-port device nonlinearity. The diagram fragments which are usually used for testing two-port devices are outlined in Fig. 6(a) (areas  $a, b$ ) using coordinates  $\{f_1, f_2\}$ . The technique for measurement of nonlinearity parameters inherent to transfer characteristics of two-port radio devices and the technique for construction of equivalent polynomial models (up to nineteenth to twenty-first order) of these characteristics are contained in the [1], [4], and [8].

Compared to conventional utilization of a spectrum analyzer for measurement of intermodulation components at the output of the two-port radio device, the use of double-frequency testing technique

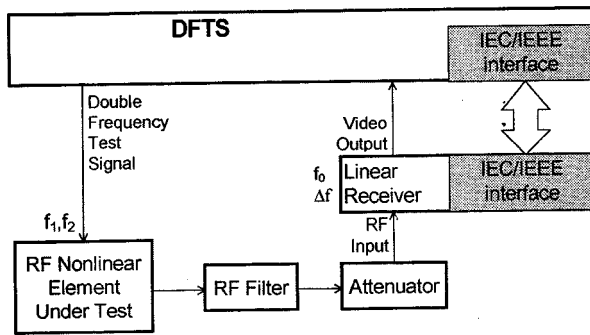


Fig. 12. Double-frequency testing of RF nonlinear elements and devices (RF & IF amplifiers, mixers, etc.).

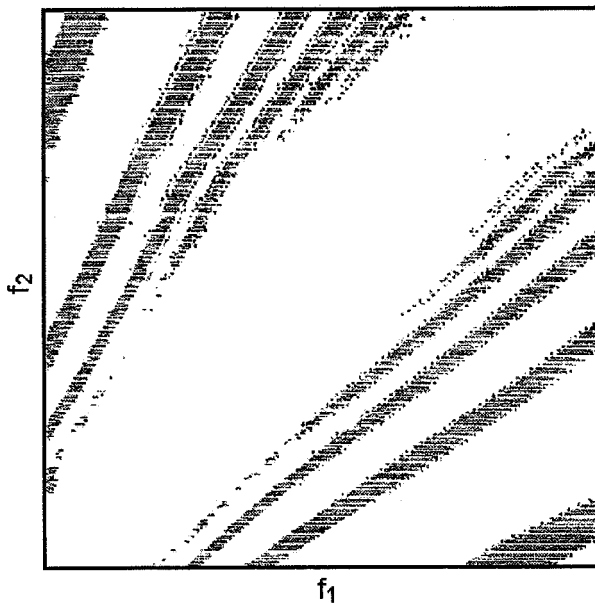


Fig. 13. Double-frequency diagram of a traveling-wave tube amplifier.

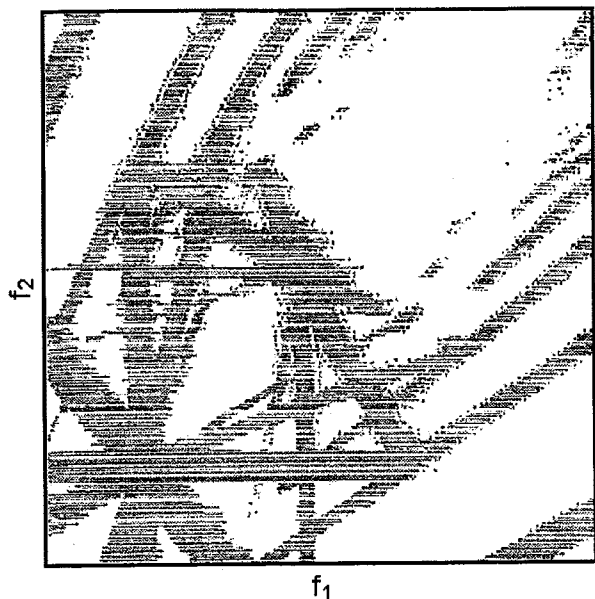


Fig. 14. Double-frequency diagram of a gunn diode amplifier.

provides a more convenient visualization of these components, thus ensuring easier identification of the spectral components. Another advantage is that it provides a method to visualize and measure specific phenomena which occur in two-port radio devices under the influence of strong interference. An example is the intermodulation generated in a two-port radio device with spurious excitation under the influence of a high-level external signal.

To illustrate, let us consider and compare double-frequency diagrams of experimental RF amplifiers in which a traveling-wave tube (TWT) and Gunn diodes are employed. These images were obtained with the use of the analog 10-GHz DFTS.

Fig. 13 shows the double-frequency diagram image of the TWT amplifier. This image contains the intermodulation components of the type  $(m+1)f_1 - mf_2$ ,  $(m+1)f_2 - mf_1$ ,  $m = 1, 2, \dots, 7$ , from the components of the third order (the widest slanted lines in the left top and right bottom parts of the image) up to components of the thirteenth to fifteenth order (lines approaching the double-frequency diagram diagonal  $f_1 = f_2$  when  $m$  is increased). The image was obtained for equal test signals frequency change ranges  $Df_1 = Df_2 = Df$  and by tuning the receiver frequency  $f_0$  approximately to  $Df/3$  below the lower test signals frequency boundaries (area  $a$  in Fig. 6(a)).

Fig. 14 shows the double-frequency diagram image of the solid-state Gunn diode amplifier. This image was obtained for the same test signals frequency change ranges  $Df_1 = Df_2$ , tuned frequency  $f_0$  and passband  $\Delta f$  of the linear receiver (Fig. 12), as used for the TWT amplifier testing. This diagram also contains the images of intermodulation components of the type  $(m+1)f_1 - mf_2$ ,  $(m+1)f_2 - mf_1$ ,  $m = 1, 2, \dots, 7$ . However, in this case, there are additional specific nodes of three-signal intermodulation on the diagonal  $f_1 = f_2$  that indicate the presence of spurious signals in the specific amplifier-under-test. Disappearance of some lines of these nodes at a certain distance from the double-frequency diagram diagonal indicates that the formation of spurious signals is of unstable character and is present only for limited (not more than 200–300 MHz) detunings  $|f_1 - f_2|$  of test signals.

### C. Testing of Radioreceivers with 2-D Panoramic Displays

When the double-frequency testing technique is applied to radioreceivers with CRT's or to other panoramic displays, e.g., radar station radioreceivers, there is a possibility of synchronizing the frequency sweeping and the display ray scanning. Thus, it is possible to obtain the double-frequency diagram image directly on the screen of the radar station display. In this case, receiver sensitivity and susceptibility at its antenna input can be determined on the basis of the threshold procedure [see (2)] as well as on images detected on the radar station screen when in a test mode.

Fig. 15 shows the double-frequency diagram image on the Tu-134 aircraft surveillance radar screen. This diagram was obtained in screen-polar coordinates  $\{\alpha, R\}$  and shows the main and image frequency channels that look like circles and dark radial bands. The structure of the circles and radial bands is determined by the form of the receiver passband frequency selectivity characteristic. The spiral images represent third order intermodulation in the main and image channels; the double flat spiral present in the second, third, and fourth quadrants of the double-frequency diagram represent second-order intermodulation in the intermediate frequency path. Visual identification of individual components on the double-frequency diagram displayed in polar coordinates may prove to be difficult. However, in general, the implementation of these tests is very simple and test diagrams enables one to detect the presence of spurious response and intermodulation paths and to characterize the paths.

Double-frequency testing of a radar receiver which employs a plan-position display or a sector display requires that the following conditions be fulfilled.

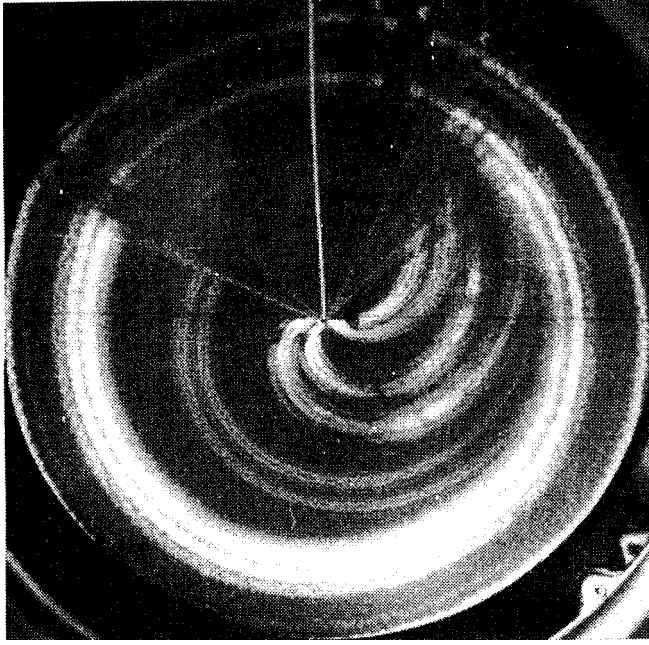


Fig. 15. Double-frequency diagram of the Tu-134 plane radar receiver.

- Initial synchronization of the radial beam sweep and frequency change of the first test signal frequency  $f_1$ ; the frequency change period  $T_{f_1}$  for this signal should not exceed the scan period  $T_R$  of the beam over the radius  $R$ :  $T_R \geq T_{f_1}$ .
- Initial synchronization of the beam sweep over the azimuth  $\alpha$  and frequency change of the second test signal frequency  $f_2$ ; the frequency change period  $T_{f_2}$  for this signal should not exceed the scan period  $T_\alpha$  of the beam over the azimuth  $\alpha$ :  $T_\alpha \geq T_{f_2}$ .
- Sweeping of test signals should be triggered by drive pulses of radial and azimuth radar display sweep.

If these conditions are fulfilled we have the possibility to display the double-frequency diagram of a radar receiver in polar coordinates  $\{\alpha, R\}$ . The possible variants of form and content of obtained diagrams and images may be studied in more detail by converting typical double-frequency diagrams shown in Fig. 6(a)–(g) into polar coordinates using the following substitutions in (3):

$$\begin{aligned} f_1 &= \frac{f_{1\max} - f_{1\min}}{R_{\max}} R + f_{1\min} \\ f_2 &= \frac{f_{2\max} - f_{2\min}}{\Delta\alpha} \alpha + f_{2\min} \\ 0 &\leq R \leq R_{\max}, \quad 0 \leq \alpha \leq \Delta\alpha \leq 2\pi \\ f_{1\max} &\leq f_1 \leq f_{1\min}, \quad f_{2\max} \leq f_2 \leq f_{2\min}. \end{aligned} \quad (10)$$

In (10),  $\Delta\alpha$ —variation range width of the beam sweep azimuth  $\alpha$ ,  $R_{\max}$ —radial beam sweep amplitude. Diagrams shown in Fig. 6(a)–(e), (g) are formed for  $f_{1\min} = f_{2\min} = 8$  GHz,  $f_{1\max} = f_{2\max} = 12$  GHz; for the diagram shown in Fig. 6(f),  $f_{1\min} = f_{2\min} = 4$  GHz.

In conclusion, we would like to note that the DFTS test signals change rate  $V_f$  is limited due to undesirable dynamic effects in the receiver-under-test or in the recording linear receiver shown in Figs. 10 and 12. These undesirable dynamic effects are similar to the known effects that are observed when signals with high frequency sweeping rate are used for measuring frequency selectivity characteristics of

narrow-band receivers. In order to evaluate the limits on the frequency change rate of test signals and on the minimum possible time of double-frequency diagram creation, it is necessary to take account of the following.

- The frequency change rate  $V_{k_1 f_1 + k_2 f_2}$  of the intermodulation oscillation of the type  $k_1 f_1 + k_2 f_2$  is  $|k_1|$  times higher than the rate  $V_{f_1}$  at which the frequency  $f_1$  of the test signal is changed and is equal to:  $V_{k_1 f_1 + k_2 f_2} = k_1 V_{f_1}$ .
- Dynamic effects may be neglected if the frequency change rates for test signals and intermodulation oscillations are not higher than  $(0.2\text{--}0.3) (\Delta f)^2$  [1], [4].
- Thus, when intermodulations up to and fifteenth to twentieth order inclusive are to be recorded, it is necessary to ensure the fulfillment of the following condition:  $V_f < (\Delta f)^2 / 30$  [Hz/sec].
- In this case, for  $N$  lines in the image of the double-frequency diagram in the ranges  $Df_1 = Df_2 = Df$ , the duration  $T_C$  of the operation cycle is determined by the relationship  $T_C > 30N \cdot Df / (\Delta f)^2$ .

It is apparent that the value of  $T_C$  for  $N = 2^7\text{--}2^8$  ranges from fractions of a second or to several seconds (when broad-band radioreceivers, one-port and two-port radio devices are tested) and up to tens of minutes (when narrow-band radio receivers are tested over a broad-frequency range).

## VI. BASIC RESULTS OF DFTS UTILIZATION

Practical experience of using the DFTS for testing of radio broadcasting, radar, radio communications, radio monitoring, and other receivers in various frequency bands has shown that

- DFTS makes it possible to significantly enhance the quality of receiver design due to timely detection and adjustment of the most undesirable paths and due to improvements in matching individual receiver elements in order to optimize the receiver design for EMC control.
- DFTS makes it possible to readily investigate the EMC cosite performance, especially for local ground-based and on-board radio systems.
- New phenomena were discovered during the utilization of the DFTS including:
  - the creation of intermodulation oscillations in generators characterized by a *nonlinear* frequency dependency [1];
  - the relationship between characteristics of spurious excitation of input receiver stages and characteristics of receiver intermodulation under a strong signal.
- DFTS allows one to use numerous methods and means of detection, identification, and measurement of parameters of objects:
  - correlation methods, input/output signal comparison methods, and geometric methods for detection and identification of objects;
  - techniques for detection and evaluation of path parameters with the use of the “noise path images”;
  - conventional methods for compressing, storing, and processing images.
- The DFTS can be implemented with a conventional modern measurement system for standard testing of receivers; in this case, only development (customization) of the DFTS software and an adequate computer to process double-frequency diagram images and run databases are required.

- The DFTS makes it possible to measure parameters of nonlinearity of input RF amplifiers of a receiver including parameters of high (fifteenth to twenty-fifth) orders [1], which make possible:
  - representation of rough (blocking, crosstalk) and more subtle (intermodulation, local oscillator noise conversion) nonlinear phenomena in a wide range of inputs;
  - utilization of “fast” EMC analysis [8], [9] using discrete models of the interference environment and the fast Fourier transform (FFT).

## VII. CONCLUSION

The author believes that the material presented above is sufficiently comprehensive to characterize the functionality enhancement of conventional equipment for two-signal testing of radio receivers, two-port radio devices (RF amplifiers, mixers, etc.) and one-port devices (generators), which may be achieved by using the principles of raster-like changing of test signals frequencies combined with visualization of test results as 2-D raster images of double-frequency diagrams. The presented technique for double-frequency testing is very efficient for extracting information about receiver susceptibility at the antenna input. This technique permits prompt detection and identification of all existing linear and nonlinear signal paths that cause interference at the receiver antenna input, which is of interest with regard to receiver system planning. The technique is especially useful at the early development stages since it enables the EMC engineer to conduct painstaking research in order to provide detailed data, thus facilitating design decisions, particularly with regard to testing receiver elements and circuits for purposes of EMC prediction.

## ACKNOWLEDGMENT

The author would like to thank Prof. A. F. Aporovitch and Prof. V. G. Ustimenko for their long-term cooperation in theoretical and experimental substantiation of feasibility of the double-frequency testing technique. He would also like to thank Prof. P. V. Matyunin for his notable contribution to the development of metrological DFTS issues in the 8–56 GHz frequency band.

## REFERENCES

- [1] A. F. Aporovich and V. I. Mordachev, “Functional possibilities of the emc characteristics monitoring of electronic apparatus by the two-frequency probing method,” in *Proc. IXth Int. Wroclaw Symp. EMC*, Wroclaw, Poland, 1988, pp. 867–872.
- [2] V. I. Mordachev and A. G. Yakubenko, “Automation of electromagnetic compatibility (EMC) radio electronic devices (RED) characteristics control by a two-frequency probing (TFP) method,” in *Proc. Xth Int. Wroclaw Symp. EMC*, Wroclaw, Poland, 1990, pp. 361–366.
- [3] V. I. Mordachev, “Automated frequency test system,” in *Proc. Vth Int. Conf. Electromagn. Interference Compat. (INCEMIC)*, Hyderabad, Andhra Pradesh, India, 1997, pp. 99–104.
- [4] V. I. Mordachev and P. V. Matyunin, Method of measuring EMC radio receiver parameters by TFP, Feb. 1990. Recommended by USSR State Committee of Radio Frequencies.
- [5] *A Handbook Series on Electromagnetic Interference and Compatibility*, D. R. J. White, Ed., Don White Consultants, Inc., Germantown, MD, 1971–1973.
- [6] U. L. Rohde, J. Whitaker, and T. T. N. Bucher, *Communications Receivers: Principles and Design*, 2nd ed. New York: McGraw-Hill, 1997, ch. 3, p. 120.
- [7] V. I. Mordachev, “Identification of image and intermodulation channels in passive radar installations,” *Problems of Signal Processing in Passive Radar Installations*, vol. 4, no. IX, pp. 3–8, 1987.

- [8] —, “Express-analysis of electromagnetic compatibility of radioelectronic equipment with use of discrete models of interference and fast fourier transform,” in *Proc. IXth Int. Wroclaw Symp. EMC*, Wroclaw, Poland, 1988, pp. 565–570.
- [9] S. L. Loyka and V. I. Mordachev, “Computer-aided nonlinear simulation at the system level,” in *Proc. Vth Int. Conf. Electromagn. Interference Compat. (INCEMIC)*, Hyderabad, India, 1997, pp. 93–98.
- [10] M. I. Skolnik, Ed., *Radar Handbook*. New York: McGraw-Hill, 1970, vol. 3, ch. 8.

## FDTD Analysis of Noise Radiation and Propagation

N. H. Younan, C. D. Taylor, and M. R. Zunoubi

**Abstract**—The analysis of effects from noise illumination of electrical and electronic systems is complicated by stochastic rather than deterministic variables. In this short paper, an analysis technique is presented for noise propagation, where the noise is modeled as a time series of discrete time impulses with amplitudes computed by a white Gaussian noise simulation. Using the noise source to simulate the drive of an appropriate antenna, the analysis of the radiated noise signal is accomplished through the use of the finite-difference time-domain (FDTD) formulation. The presented technique is verified by a comparison with the results obtained from using the method of moments and a wire antenna radiator. In addition, limitations, stability, and applicability of the presented formulation are discussed.

**Index Terms**—FDTD, noise modeling, radiation.

## I. INTRODUCTION

Modern electronic systems and devices are rapidly decreasing in size and operating at lower and lower voltages. As a result, noise vulnerability has become increasingly more important. The analysis of effects from noise illumination is often complicated by stochastic rather than deterministic variables and by nonlinear responses, i.e., responses involving terminal protection devices, magnetic shielding, rectification, etc., and by the presence of anisotropic materials such as composites. Generally, a simple analytical analysis is not possible. However, with the advent of ready access to high-performance computing, numerical modeling of electromagnetic effects is a viable option in both design and analysis.

Introduced first by Yee [1], the finite-difference time-domain (FDTD) technique has been proven to be a convenient and effective tool for time-domain analysis of various electromagnetic problems including anisotropic and nonlinear materials and devices. Recently, Zunoubi *et al.* [2] have demonstrated that the FDTD technique can be efficiently used to determine the radiation from an antenna driven from a discrete time impulse source. Therefore, it is possible to use the FDTD method to determine radiation from an antenna driven from a time series of discrete time impulses.

In order to analyze noise radiation and propagation, the output from a noise source is modeled as a time series of discrete time impulses

Manuscript received September 8, 1998; revised January 26, 2000.

N. H. Younan and C. D. Taylor are with the Department of Electrical and Computer Engineering, Mississippi State University, Mississippi State, MS 39762 USA.

M. R. Zunoubi was with the Center for Computational Electromagnetics, University of Illinois, Urbana, IL 61801 USA. He is now with the Department of Electrical and Computer Engineering, Lake Superior State University, Sault Ste. Marie, MI 49783 USA.

Publisher Item Identifier S 0018-9375(00)04688-3.